ENCIT 2018

ABCM Associação Brasileira de Engenharia e Ciências Mecânicas

17th Brazilian Congress of Thermal Sciences and Engineering
November 25th-28th, 2018, Águas de Lindóia, SP, Brazil

# ENCIT-2018-0337
# DEVELOPMENT OF A PARTICLE TRACKING VELOCITY MEASUREMENT TECHNIQUE FOR THE STUDY OF GAS-LIQUID FLOWS WITH DIFFERENT INTERFACIAL LENGTH SCALES IN VERTICAL PIPES

**Rafael F. L. de Cerqueira**
**Emilio E. Paladino**
**Clovis R. Maliska**

SINMEC - Computational Fluid Dynamics Lab Mechanical Engineering Department, Federal University of Santa Catarina, 88040-900 - Florianopolis - SC - Brazil
rafaelfc@sinmec.ufsc.br, paladino@sinmec.ufsc.br, maliska@sinmec.ufsc.br

***Abstract.*** *The present work aims the development of a Particle Tracking Velocimetry (PTV) technique capable to identify and then track the motion of the different gas phase spatial structures present on gas-liquid vertical flows. Due to its transient and strong spatial variations, the vertical slug flow pattern is studied, since the gas phase are spatially distributed as dispersed small bubbles or large elongated bubbles, which are commonly referred as Taylor bubbles. The different morphologies can be classified on two groups: i) small scale interfacial scale phase, the dispersed bubbles and ii) large scale interfacial scale phase, the Taylor bubble. This morphological classification arises from the different length of the gas phase structures presented on the flow pattern. In order control the interfacial length scales and test out the proposed method, the real slug flow is simplified to a "quasi-slug" flow pattern, where a fabricated flow pattern is created by the injection of Taylor bubble into gas-liquid bubbly vertical flow, where it is possible to vary the Taylor bubble length and the of the bubbly flow liquid and gas superficial velocities, simulating a real slug flow pattern. The Particle Tracking Velocimetry implementations found on literature can only be used for flows with a single interfacial length scales, such as the rising of a Taylor bubble or the individual tracking of dispersed bubbles found on gas-liquid bubbly flows. The proposed method consists on two different tracking algorithms that are coupled to be used on a gas-liquid flows with different interfacial length scales, being able to track the motion of the different interfacial length scales and also extract information about its shape and size.*

***Keywords:*** *Particle Tracking Velocimetry, PTV, Taylor bubble, bubbly flow, slug flow*

## 1. INTRODUCTION

Gas-liquid two-phase flows occur in a great variety of natural phenomena and technical processes. Despite its frequent occurrence, the measurement of two-phase gas-liquid flows has been a challenging task for scientists and engineers. Due to the strong spatial variations and high transient behavior, averaged based models are used in engineering applications for the machine and system design. Hence, those models rely on experimental techniques which can return consistent averaged spatial and/or temporal flow variables. Additionally, some experimental techniques can be used to acquire local and/or instantaneous measurements which can be used to gain insight into the complex gas-liquid flow phenomena.

Among the flow patterns encountered for gas-liquid flows in ducts, the slug pattern has drawn special attention of researchers mainly because of its intermittent characteristic which, in oil production systems, can be associated to difficulties in control system operations due to the strong pressure and velocity fluctuations and system damage in the case of sever slug conditions. Additionally, this intermittent characteristic brings additional difficulties in measuring flow variables for this flow pattern. The slug flow in vertical ducts consists of long bullet shaped bubbles, called Taylor bubbles, followed by liquid slugs, typically, containing dispersed small bubbles. The region between the nose of one Taylor bubble and the b of the subsequent one is called slug unit, and the whole flow can be outlined as a sequence of several slug units. As Taylor bubbles travel faster than the liquid phase, the liquid is displaced and flows back through a thin film around the Taylor bubble. This film expands at the bubble rear, generating a recirculation pattern. The length and intensity of these recirculations can be associated with global flow parameters, as Taylor bubble velocity and heat and mass and transfer coefficients in the liquid slug region.

Besides, the transfer coefficients at the Taylor bubble nose and film, are also associated with the velocity profiles in those regions. Thus, in order to get a deeper insight of this flow pattern, several researchers presented experimental studies and techniques aiming the detailed measurement of the flow fields around Taylor bubbles, most of them using Particle Image Velocimetry (PIV) (Polonsky *et al.*, 1999; Bugg and Saad, 2002; Van Hout *et al.*, 2002; Nogueira *et al.*, 2003, 2006; Meneghini *et al.*, 2014). Nevertheless, these works consider a very simplified figure of the flow around Taylor bubbles, particularly, when compared with the flow of these bubbles in real slug flow. Additionally, those experimental studies focused on liquid phase measurement, mainly characterizing the flow around Taylor bubbles.

From the slug flow pattern perspective, the gas phase can be classified on two groups: i) the dispersed bubbles, with a small interfacial length scale and ii) the Taylor bubble, with a large interfacial length scale. Several authors presented experimental techniques focused on the characterization of the gas phase on gas-liquid flows (Honkanen *et al.*, 2005; Xue *et al.*, 2012; Lau *et al.*, 2013; Fu and Liu, 2016; Acuña and Finch, 2010), which are specifically focused on gas-liquid vertical bubbly flows. These works use PTV (Particle Tracking Velocimetry) methods to track the dispersed bubbles on the flow and then compute its shape, size, and velocity distributions.

For the Taylor bubble tracking, Polonsky *et al.* (1999) tracked the motion of a Taylor bubble rising on a vertical duct, capturing its shape and length, correlating the nose and bottom frequency oscillation with the liquid flow conditions. The experiments in Polonsky *et al.* (1999) describe the flow of a Taylor bubble on a liquid stream, ignoring the dispersed bubbles that are present on a real slug flow.

Mayor *et al.* (2007) developed an image processing technique, capable of tracking the motion of the Taylor bubbles in different slug flow pattern conditions, extracting from a series of video frames information about the Taylor bubbles dimension, velocity, and distance. However, the tracking algorithm described on Mayor *et al.* (2007) does not track the motion of the small interfacial length scale gas phase, neglecting the dispersed bubbles individual motion on the region between the nose of one Taylor bubble and the bottom of a subsequent one.

This paper presents a PTV based technique for the study of the gas-liquid flows in different interfacial length scales in vertical pipes. In order to reproduce a flow with different interfacial length scales, a "quasi-slug" flow pattern (Meneghini *et al.*, 2014) is studied, in which dispersed bubbles are injected into the flow containing a liquid phase and a Taylor bubble, where the gas and liquid flow rates can be controlled, resulting on gas phase structures similar to those found on real slug flow patterns.

The PTV algorithm proposed for the dispersed bubbles in this work is based on similar implementations found in literature (Honkanen *et al.*, 2005; Xue *et al.*, 2012; Lau *et al.*, 2013; Fu and Liu, 2016; Acuña and Finch, 2010), but some corrections on the image analysis method are proposed to deal with bubble shadows superposition when the images are acquired with back-light illumination. Most of the PTV implementations are focused on analyzing the flow inside narrow channels and/or reduced gas void fraction values (less than $1.0\%$). In these cases, bubble shadows overlap is not a critical problem. In the case of the present work, the technique is applied on small diameter ($D$ =26.2 mm) pipe with void fractions up to $11.4\%$. For the Taylor bubble tracking the technique described in Mayor *et al.* (2007) will be used to track the motion of the large interfacial length scales, while the extraction of the Taylor bubble nose is performed using the methods described in Polonsky *et al.* (1999). The two bubble tracking techniques are implemented on the same numerical framework, extracting spatial and transient information from the two different gas phase structures (dispersed and Taylor bubbles) found on the "quasi-slug" flow pattern from high speed camera images.

## 2. METHODOLOGY

### 2.1 Experimental setup

This section describes the experimental setup used in this work. This system allows for the generation of a single-phase liquid stream, bubbly flow, real and "quasi" (Meneghini *et al.*, 2014) slug flow in a straight vertical duct, where the water and air flow rates, and thus, the superficial velocities, can be independently controlled.

The experimental apparatus is schematically depicted in Fig. 1a). The test section consists of a transparent pipe with $D = 26.2$ mm internal diameter and $L = 2.0$ m length.

At the PIV measurement section, a box constructed with transparent acrylic, made with 8 plane faces, filled with the water is included to minimize optical distortion. A two-phase stream is generated at the bottom of the test section by combining a liquid stream (tap water), driven by a centrifugal pump, and air from the compressed air line from the building. To eliminate oil and solid particles, air is treated and pressure is maintained constant at the injection point through a pressure regulating valve, making it independent of the line demand. The dispersed bubbles are injected at the bottom of the tube, and the gas superficial velocity is measured by two OMEGA FL-3802ST/FL-3861SA flow meters with ranges of 81.4-814.0 standard mL/min and 26.3-263.0 standard mL/min, both with $\pm 2.0\,\%$ full scale accuracy. The flow rate is controlled by a needle valve downstream. In order to correct the gas superficial velocity due to gas expansion, a pressure and a temperature sensors were installed downstream the needle valves. As the return to the reservoir consists of a relatively short ($\sim 0.5$ m), and $50.0$ mm internal diameter duct, and the reservoir is opened to the atmosphere, it was assumed that the pressure at the test section was close to the atmospheric pressure. The water flow rate is measured by an OMEGA FL46303

flow meter with range of 1.00-7.50 l/min with $\pm 5.0\,\%$ full scale accuracy. The liquid flow rate is controlled through a frequency inverter connected to the electric water pump motor.

As a way of facilitating the study of slug flow, it has been chosen not to study the real flow this pattern, but rather a fabricated flow pattern in which dispersed bubbles are injected into the flow containing a liquid phase and a Taylor bubble, where the gas and liquid flow rates can be controlled (Meneghini *et al.*, 2014).

The dispersed bubble generation system is shown in Fig. 1a), which consists of the compressed air filter, a flow regulator, a pressure regulator, a pressure gauge and an air flowmeter. In the injection of dispersed bubbles, the gas phase (compressed air) is conducted to the vertical duct through a separated piping line. At the end of the piping line there is an air diffuser that allows the production of dispersed bubbles, which in turn enters the acrylic duct with internal diameter of 26.2 mm.

The Taylor bubble is injected by a system formed by a reservoir with known volume, which has at its two ends, solenoid valves electronically actuated. From the pressure of the compressed air line, it is possible to control the volume of the Taylor bubble to be injected, since the reservoir has a constant volume. An electronic system controls the injection cycles of the Taylor bubbles, from the valve opening and closing command.

Initially, the valve 1 opens, filling the reservoir with known volume with compressed air at a given pressure. After a certain time, the valve 1 is closed for equalization of the system pressure and the initially closed valve 2 is actuated, releasing the volume of air that is led by a hose to the liquid filled duct, becoming a bubble of Taylor. In order to improve the injection cycles, the valves opening and closing instants ($t_1$ e $t_2$), as well as the time necessary to stabilize the process in the air reservoir ($t_{stab.}$) and the waiting time between the different generation cycles ($t_{wait}$), were electronically controlled.

For the synchronization between the passage of the Taylor bubbles and the acquisition through the high speed camera, the technique developed in Meneghini *et al.* (2014) has been optimized for the detection of the passage of Taylor bubbles in systems with a high amount of gas ($\alpha_g > 10\%$) and modified to be used with a high speed camera system.

For the bubble tracking algorithm, a bright white LED array is added at the back of the test section shown in Fig. 1. A CCD digital high speed camera (Redlake MotionPro X3) with 52mm lens was used to acquire the flow images using the LED illumination array, the images were recorded in 256 grey scale levels with image size of 1024 x 1024 pixels with a frame rate of 800 fps. An schematic of the camera and illumination arrangement for the image acquisition used by the bubble tracking algorithm is depicted in Fig. 1b).

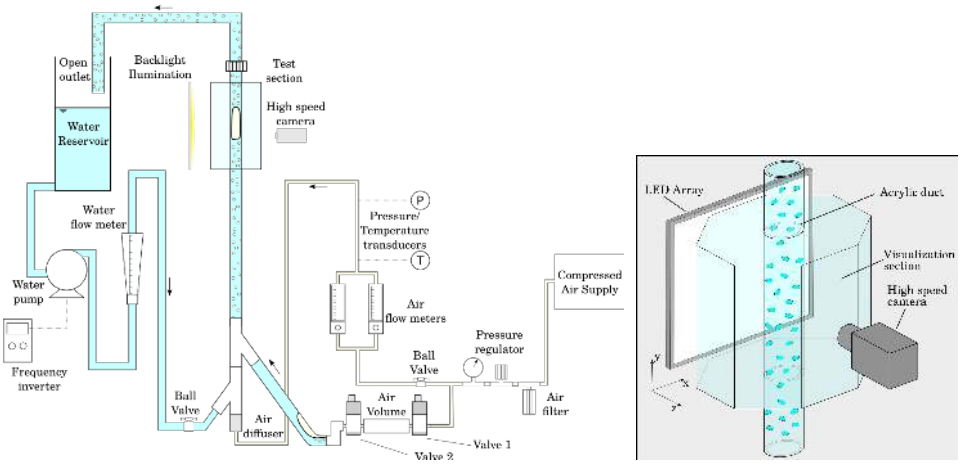


(a) (b)

Figure 1: Schematic of: a) the experimental setup and b) the camera and illumination arrangement for the image acquisition used by the bubble tracking algorithm.

The backlight illumination shown in Fig. 1b) produces images with high contrast between the liquid and gas phases. Figure 2 shows some typical high speed camera images obtained with the backlight illumination arrangement, for different gas and liquid superficial velocities, where the contrast difference enables the visual discrimination of the two phases.

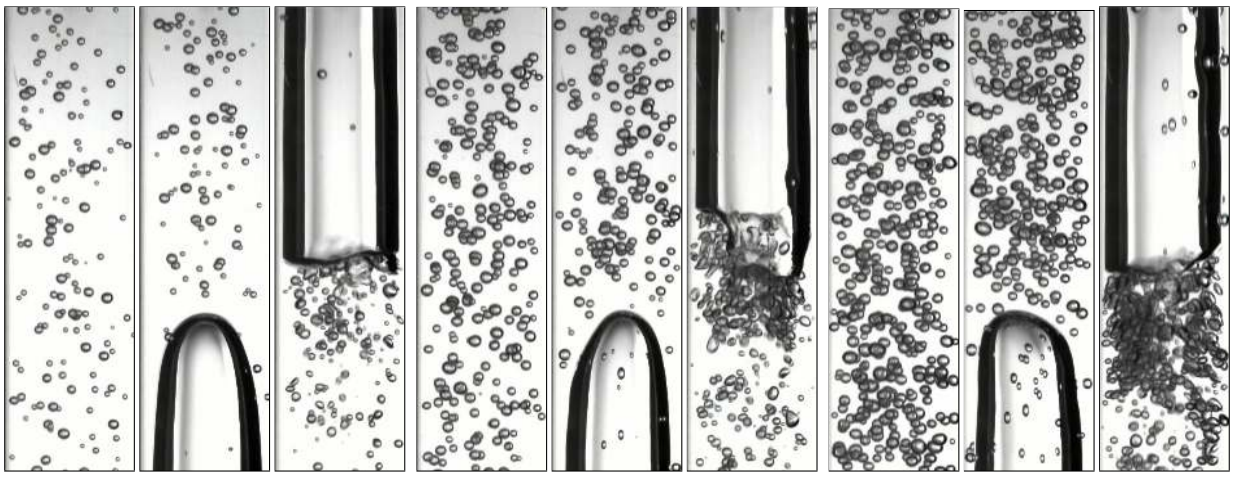

(a) (b) (c)

Figure 2: Typical high speed cameras obtained with the backlight illumination arrangement for different flow stream configurations for $j_l$ = 21.64 $\times 10^{-2}$ m/s and: a) $j_g$ = 2.38 $\times 10^{-3}$ m/s and $\alpha_g$ = 0.7 %; b) $j_g$ = 13.55 $\times 10^{-3}$ m/s and $\alpha_g$ = 3.5 %; c) $j_g$ = 19.83 $\times 10^{-3}$ m/s and $\alpha_g$ = 4.9 %. The images sequentially shown the Taylor bubble passage in the "quasi-slug" fabricated flow pattern, where the Taylor bubbles are injected into a controlled $j_l$ and $j_g$ bubbly flow stream.

### 2.2 Dispersed bubble tracking

As can be seen in Fig. 2, it is observed that, in general, the dispersed bubbles do not always have an ellipsoid/circular shape and, in several cases, bubble shadows overlapping occurs. The disturbances in bubbles shape are originated from the bubble-bubble interaction and the liquid phase turbulence, and for larger bubbles due to inertial effects. These disturbances also affect the bubbles motion, causing some bubble clustering and subsequent overlapping in the projected image plane. However, in some cases, the bubble "clustering" appearing in the recorded images is not a physical feature of the flow, but a consequence of the projection of the recorded bubbles in the image plane, in virtue of the use of back-light illumination in pipe flows. In fact, the observed clustering and overlapping also happen with bubbles that are distant from each other in the direction of the projection axis ($z$), which also causes ambiguities in the bubbles motion in the radial direction ($x$ direction in Fig. 1b)).

Due to the difficulties associated with the bubble identification in these cases, the method developed in Cerqueira *et al.* (2018) was used to identify and track the dispersed bubbles. In order to overcome the bubble clustering (or shadows projections overlapping) in cases with moderate or high void fractions, the method is based on two different processing techniques. The first technique captures the bubble outlines and is capable of determining the dispersed bubbles' velocity and diameter. The second technique is based on the internal bubble contours tracking, which is not capable of capturing bubble shapes and sizes but can measure the dispersed bubbles velocities. Hence, for low void fractions the method described in Cerqueira *et al.* (2018) can accurately capture the dispersed bubble size and velocity, while for high void fractions, most of the tracked bubbles do not have information about its size, but only its instantaneous rising velocity. Figure 3 shown the final result of the method described in Cerqueira *et al.* (2018) for different bubbly flow configurations, illustrating that for low void fraction bubbly flow most of the bubble contours are captured, and the for the cases with higher void fraction values, only the instantaneous velocity vectors are captures.

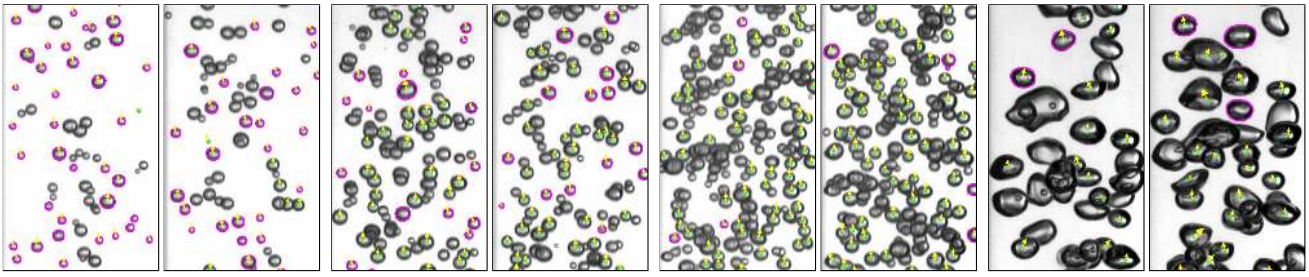

(a) (b) (c) (d)

Figure 3: Example of the dispersed bubble tracking algorithm for different flow stream configurations: a) $j_l$ = 21.64 $\times 10^{-2}$ m/s, $j_g$ = 2.38 $\times 10^{-3}$ m/s and $\alpha_g$ = 0.7 %; b) $j_l$ = 21.64 $\times 10^{-2}$ m/s, $j_g$ = 13.55 $\times 10^{-3}$ m/s and $\alpha_g$ = 3.5 %; c) $j_l$ = 21.64 $\times 10^{-2}$ m/s, $j_g$ = 19.83 $\times 10^{-3}$ m/s and $\alpha_g$ = 4.9 % and d) $j_l$ = 0.0 $\times 10^{-2}$ m/s, $j_g$ = 19.83 $\times 10^{-3}$ m/s and $\alpha_g$ = 11.0 %.

### 2.3 Taylor bubble tracking

In order to identify the Taylor bubble on the acquired high-speed images, the procedure described by Mayor *et al.* (2007) and illustrated in Fig. 4 is applied. As seen in Fig. 4, the image processing algorithm allows the exact identification of the Taylor bubble nose and bottom position and the nose shape coordinates in a specified frame.

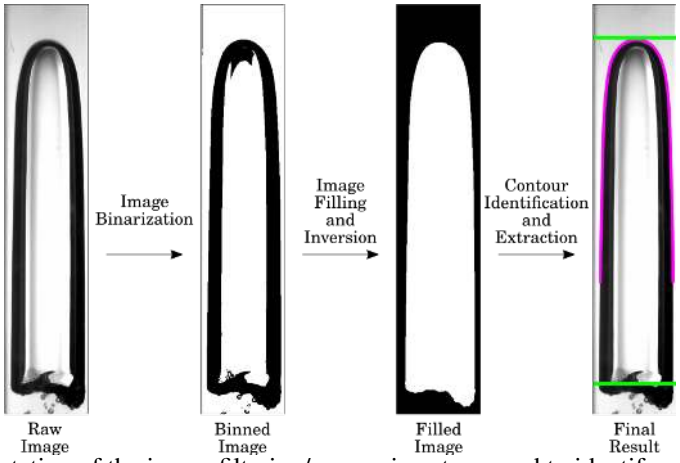


Figure 4: Schematic representation of the image filtering/processing steps used to identify a Taylor bubble from the high speed camera acquisitions.

Due to the presence of the dispersed cases in the Taylor bubble wake region, the procedure fails in some cases. Examples of this problem in the binarization step can be seen in Fig. 5, where the filling/inversion operation fails to acquire a closed contour inside the Taylor bubble.

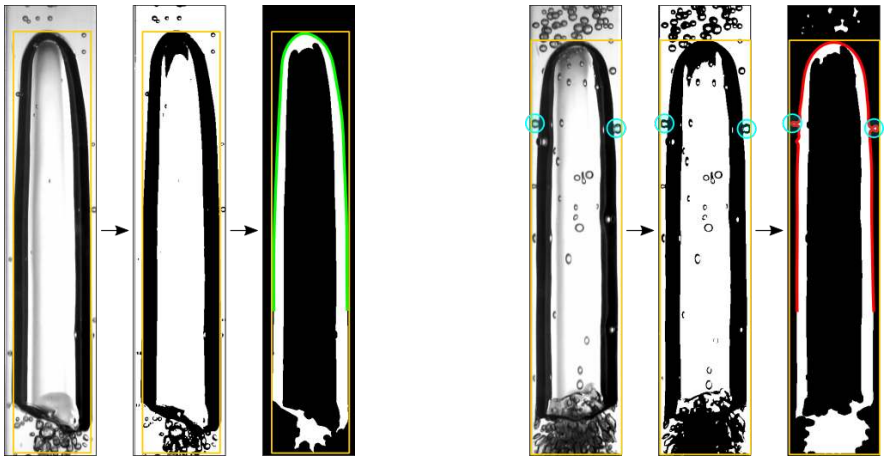

(a) (b)

Figure 5: Binarization and filtering problem caused by the presence of the dispersed bubbles in the wake region for different flow configurations: a) $j_l$ = 21.64 $\times 10^{-2}$ m/s, $j_g$ = 2.38 $\times 10^{-3}$ m/s and $\alpha_g$ = 0.7 %; b) $j_l$ = 21.64 $\times 10^{-2}$ m/s, $j_g$ = 19.83 $\times 10^{-3}$ m/s and $\alpha_g$ = 4.9 %. The images also show the extracted nose shape, highlighting the presence of a dispersed bubble in the liquid film region in b).

In Mayor *et al.* (2007) the authors apply an additional erosion filter to "filter out" the dispersed bubble in the region and hence define the Taylor bubble bottom position. However, since the additional erosion filter was not capable of removing this spurious contribution from the Taylor bubble images, an alternative method was used to define the bottom position. The method is used when the procedures described in Mayor *et al.* (2007) fails and is based on the pixel intensity profile along the bounding rectangle's center which encloses the largest contour of the filled image, as seen in Figs. 5 and 6. Figure 6a) illustrates the method, which shows the average pixel distribution on the highlighted area and the corresponding nose and bottom position project on the raw high-speed camera images.

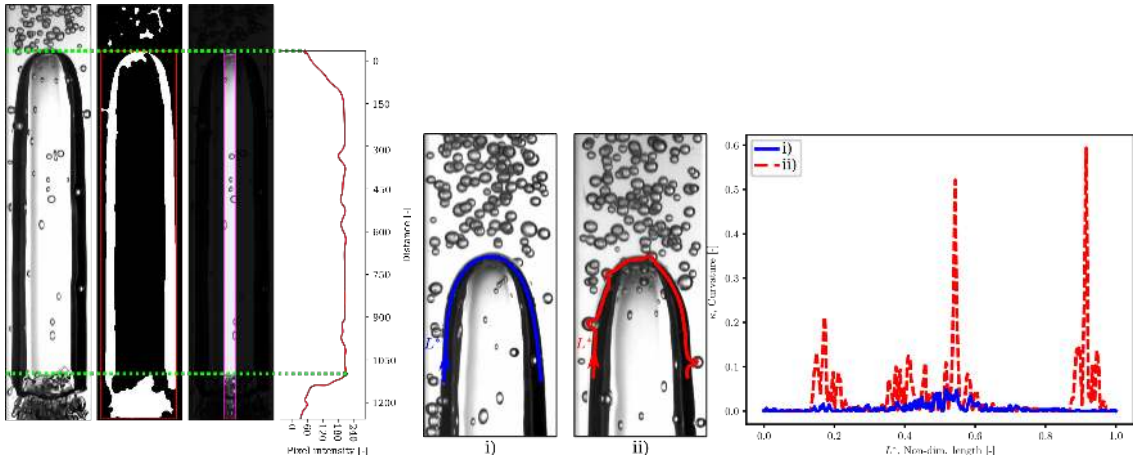


(a) (b)

Figure 6: a) Schematic representation of the image filtering/processing steps used to identify a Taylor bubble from the high speed camera acquisitions. b) Local curvature analysis around the Taylor bubble outline, illustrating multiple curvature ($\kappa$) peaks due to the presence of a dispersed bubbles.

For the bubble nose shape extraction, the external contour outline of the filled image is used. To avoid problems associated with the dispersed bubbles in the liquid film, only the contour outline below a certain distance of the nose is extracted, while the remaining is discarded. Additionally, since dispersed bubbles penetrate the liquid film, it is necessary to perform a curvature analysis in the extracted Taylor bubble nose shape coordinates, since its presence affects the binarization step in this region. Figure 6b) illustrates a bubble outline for two cases, where it is possible to visualize the curvature peak due to the presence of dispersed bubbles on the liquid film. In order to classify a nose outline as valid or not, a simple threshold parameter is used, i.e., if the local curvature is above this threshold value, its outline is discarded. In Fig. 5 this is shown by the red and green nose shape outlines, where the green is classified as a valid Taylor bubble (Fig. 5a)) outline and red is discarded (Fig. 5b)).

Figure 7 shows the Taylor bubble nose shape outline and the bottom and nose position in different times instants for a "quasi-slug" flow regime with a void fraction of $\alpha_g$ = 4.9 % ($j_l$ = 21.64 $\times 10^{-2}$ m/s and $j_g$ = 19.83 $\times 10^{-3}$ m/s).

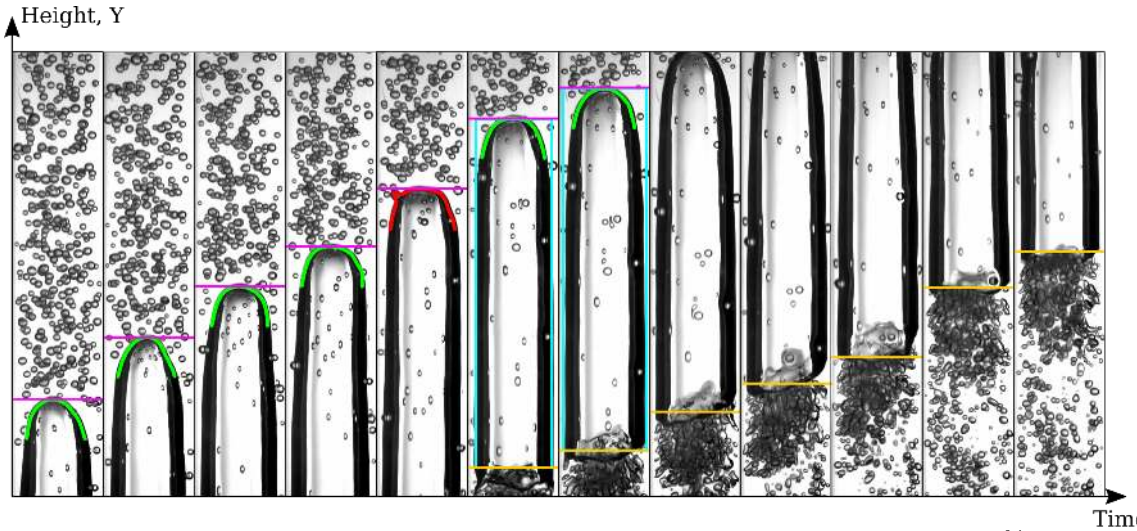


Figure 7: Taylor bubble rising motion in the "quasi-slug" flow regime with a void fraction of $\alpha_g$ = 4.9 % ($j_l$ = 21.64 $\times 10^{-2}$ m/s and $j_g$ = 19.83 $\times 10^{-3}$ m/s). For this example, due the presence of dispersed bubbles, the method only analyzed the nose contours with a maximum height of $0.5D$.

From the bottom and nose position in different time instants, it was possible to compute the Taylor bubble nose and tail velocities in a single experiment and also define its length. A visual demonstration of this procedure can be seen in Fig. 8, where the linear slope approximation results in the Taylor bubble rising velocities. It is important to state that for the cases with dispersed bubbles, such as the one shown in Fig. 8, that it is not possible to acquire the nose and bottom position all the analyzed frames. Thus, the points in Fig. 8 are not continuous samples.

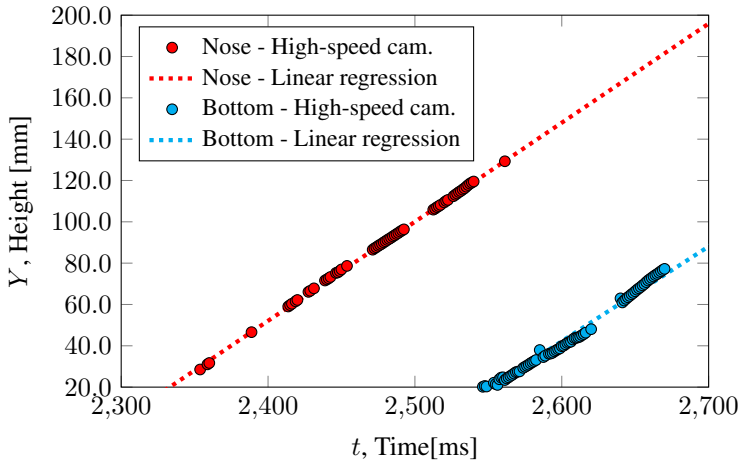


Figure 8: Taylor bubble nose and bottom position from the high-speed camera images in different time instants for the $j_l$ = 21.64 $\times 10^{-2}$ m/s, $j_g$ = 19.83 $\times 10^{-3}$ m/s and $\alpha_g$ = 4.9 % flow condition. The filled points represent the data obtained from the developed algorithm and the dotted lines its linear fit regression.

### 2.4 Coupled Tracking Algorithm

Figure 9 shows the coupled dispersed and Taylor bubble tracking from two different "quasi-slug" flow configurations, distinguishable by the size of the dispersed bubbles in each case. As seen, the coupled algorithm is capable of identifying and tracking the different length scale interfaces correctly. Additionally, as shown in Fig. 9, the dispersed bubbles in the liquid film are not tracked by the algorithm. This modification is necessary due to the image projection of the shadowgraphy method. Since the bubbles are projected into the image plane, the dispersed bubbles positioned "behind" the Taylor bubble are optically distorted by the latter. Hence, since the method was not designed to distinguish between the valid and optically distorted bubbles of the liquid film, the bubble tracking is deactivated in this particular region. In order to deactivate the dispersed bubble tracking, the information about the nose and bottom position are used to create a non-tracking zone. So, if the dispersed bubble is between these two positions, the bubble tracking is deactivated. Since it is not possible to acquire the two positions in the entire frames of a single acquisition, due to the reasons mentioned in the paragraphs above, the information of the linear regression (see Fig. 8) is employed.

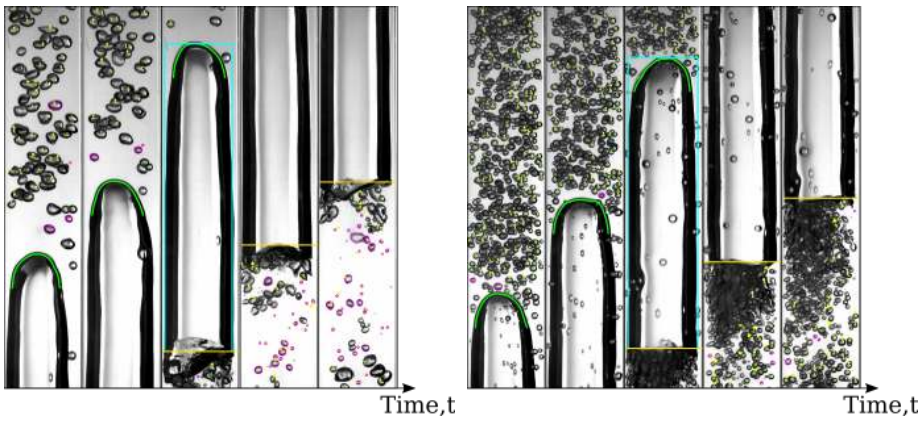


(a) (b)

Figure 9: Image sequence of a "quasi-slug" flow, where the Taylor bubble is identified from the high speed camera images and the proposed method capture its nose shape and the bubble length. The velocity vectors and contour outline of the dispersed bubbles are captured before, after and during the Taylor bubble passage on the test section. The bubbly flow stream of the "quasi-slug" cases corresponds to: a) $j_l$ = 0.0 m/s, $j_g$ = 13.55 $\times 10^{-3}$ m/s and $\alpha_g$ = 7.1 % – b) $j_l$ = 3.64 $\times 10^{-2}$ m/s, $j_g$ = 19.83 $\times 10^{-3}$ m/s and $\alpha_g$ = 11.0 %.

Since the coupled tracking algorithm allows the tracking of the different interfacial lengths of the manufactured "quasi-slug" flow, the instantaneous axial distances from the Taylor bubble nose and bottom is readily available. Hence, it was possible from the original Lagrangian frame of reference, perform statistical analysis of the dispersed bubbles around the Taylor bubbles in a Eulerian frame of reference. Figure 10 exemplifies the "Lagrangian-to-Eulerian" transformation, by illustrating the rising motion of a Taylor bubble in two time steps. In Fig. 10, the method is shown only for the Taylor

bubble bottom, since the procedure using the bubble nose is analogous. First, as soon the nose position is localized, the image is "discretized" in small rectangular cartesian regular cells, as shown by operation A of Fig. 10. After this discretization step, if a dispersed bubble is found, the nearest cell of the bubble centroid is pointed to that particular cell. In this operation, given by operation B of Fig. 10, the bubble properties ($u_g, v_g, d_eq$) are pointed on a global hold processor. The global hold processor is shown by the grid shown in Fig. 10c). As seen in Fig. 10, care is taken to deal with the different Taylor bubble bottom position as the bubble rises.

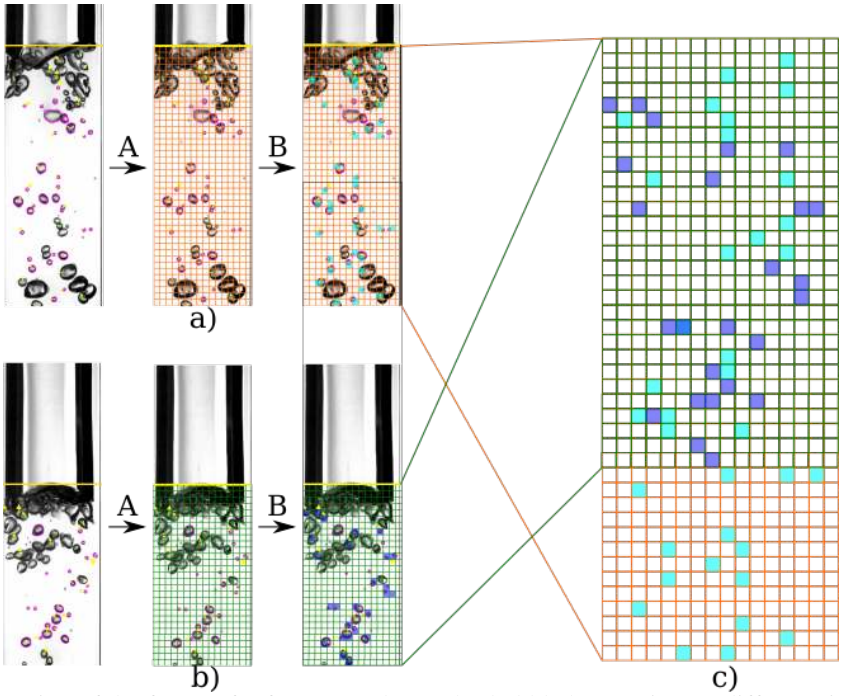


Figure 10: Transformation of the frame of reference at the Taylor bubble bottom in two different time steps (a) and b)).

After transforming the frame of reference from Lagrangian to Eulerian, the dispersed bubble ensemble averaged properties can be readily computed as,

$$\langle \Phi(x,y) \rangle = \frac{\sum_{i=0}^{N_{\text{hold}}} \Phi_i(x,y)}{N_{\text{hold}}} \tag{1}$$

where $N_{\text{hold}}$ is the number of bubbles acquired in a (x,y) position through the frame of reference transformation discussed in the above paragraphs. The $N_{\text{hold}}$ is not a constant value throughout the Eulerian field, which is different from cell to cell. The $\Phi$ dispersed bubble properties are the x-velocity ($u_g$), y-velocity ($v_g$) and equivalent diameter ($d_{eq}$). For each experiment, at least 45 bubbles were filmed in 400 fps, hence assuring a large number of $N_{\text{hold}}$ through the whole Eulerian field.

## 3. RESULTS AND DISCUSSION

### 3.1 Effect of the dispersed bubbles on the Taylor bubble rising velocity

Figure 11 presents the ensemble averaged Taylor bubble rising velocities $\langle U_{tb,N} \rangle$ measured through the high-speed camera image analysis, for different dispersed gas volume fraction and different liquid superficial velocities. The parameter $\alpha_g$ in the abscissas represents the volume fraction of dispersed bubbles, not the total volume fraction. Each point in Fig. 11 was averaged with at least 45 samples, i.e., Taylor bubbles with an approximate length $L_{tb}$ of $3.8D(\langle L_{tb} \rangle \approx 100.0$ mm). Two different trends are observed in those curves. For the stagnant flow conditions, Fig. 11a), the Taylor bubble rising velocity increases linearly with $\alpha_g$, showing some sort of "slope" discontinuity near the $5.0 \leq \alpha_g \leq 8.0$ region, indicating some sort of flow transitioning around those values. As discussed in the next sections, this transitioning effect is closely related with the dispersed bubbles ahead of the Taylor bubble. For the co-current liquid flow cases, Figs. 11b) and c), the Taylor bubbles rising velocity is increased by the presence of dispersed bubbles and the, for higher $\alpha_g$, this velocity decreases, maintaining, however, values higher than the case without dispersed bubbles. These results clearly indicate that the presence of dispersed bubbles in liquid the slugs, will affect the whole flow structure around Taylor bubbles and this effect should be taken into account in the study of real slug flows.

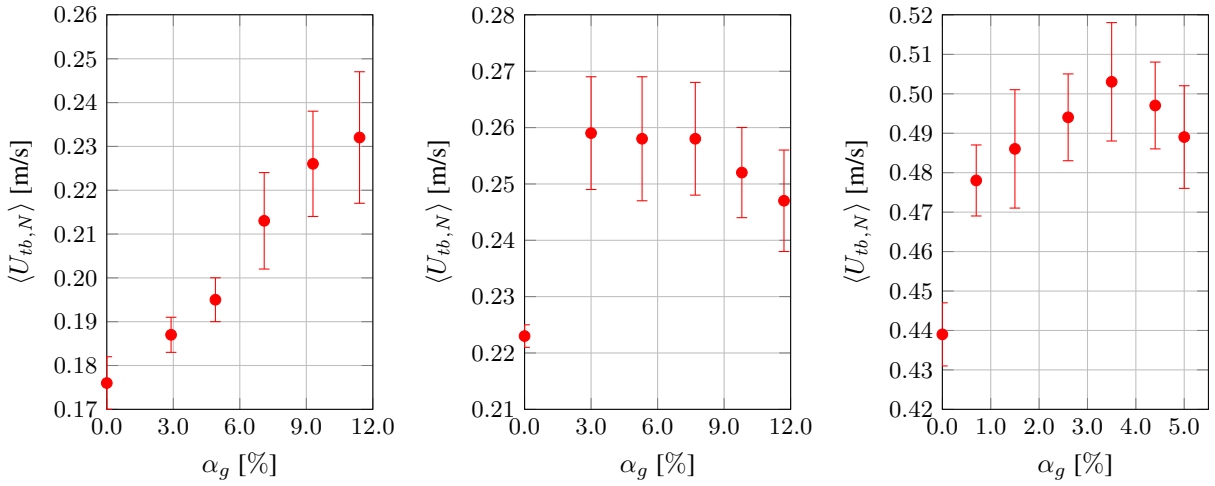


(a) $j_l = 0.0$ m/s (b) $j_l = 3.09 \cdot 10^{-2}$ m/s ($Re_l = 812$) (c) $j_l = 21.64 \cdot 10^{-2}$ m/s ($Re_l = 5684$)

Figure 11: Influence of the dispersed gas volume fraction on the Taylor bubble nose tip velocity for different "quasi-slug" flow regimes. The error bars represents the ensemble standard deviation.

### 3.2 Dispersed bubbles analysis around Taylor bubbles

From the couple tracking developed algorithm, it was possible to analyze the ensemble averaged dispersed bubble flow around Taylor bubbles. It is important to state this sort of "two-dimensional" analysis have only a qualitative value, since due the aforementioned bubble projection, it is not possible to discriminate the bubbles in the z-direction. However, despite its limitations, those results are important to gain insight of the flow around the Taylor bubbles. Thus, those ensemble averaged fields can be used to understand the influence of the dispersed gas volume fraction on the Taylor bubble nose tip velocity seen in Fig. 11.

Figure 12 shows the $\langle v_g \rangle$ filled contour plots behind the Taylor bubble.

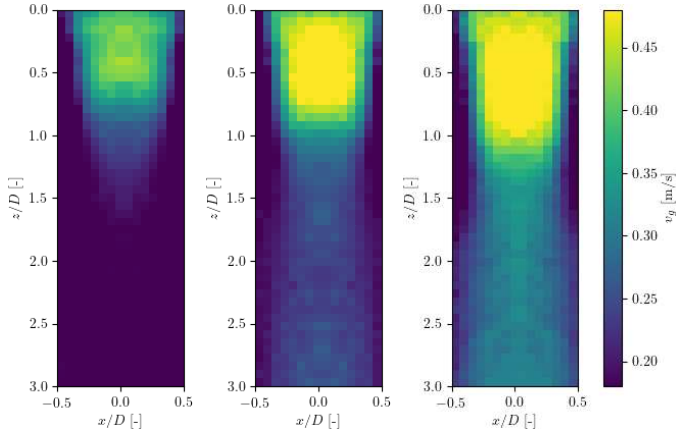


(a) (b) (c)

Figure 12: Contour plots of the vertical (y-direction) $\langle v_g \rangle$ dispersed bubble rising velocity for $j_l = 21.64 \cdot 10^{-2}$ m/s: a) $j_g = 5.89 \cdot 10^{-3}$ m/s and $\alpha_g$ = 1.5 %; b) $j_g = 13.55 \cdot 10^{-3}$ m/s and $\alpha_g$ = 3.5 %; c) $j_g = 19.83 \cdot 10^{-3}$ m/s and $\alpha_g$ = 4.9.%.

The contour plots of Fig. 12 that the void fraction alters significantly the flow behind the Taylor bubble. As shown, there is an increase in the magnitude of the dispersed bubble velocities in the wake region. Additionally, the region where the recirculation is stronger ($v_g > 0.40$ m/s) increases with the void fraction. It is possible that the dispersed bubbles motion on the wake, increase the total drag around the Taylor bubble, hence increasing the rising velocity. However, as shown in Fig. 12, the increase in the rising velocity is up to a certain void fraction value, decreasing after this point. As observed in the high-speed camera footage, this decrease is associated with the bubble tip nose lateral movement and dispersed and Taylor bubble collisions. For the cases with a higher void fraction, the Taylor and dispersed bubble collision are more frequent, slowing its rising movement. Also, those footages also show that the turbulent wakes from the dispersed bubbles deform the Taylor bubble nose tip, hence producing a lateral motion, for the cases with higher void fraction ($\langle \alpha_g \rangle$ >3.0 in Fig. 11c).

## 4. Final Remarks

A PTV (Particle Tracking Velocimetry) was developed to track the large and small interfaces length scale of gas-liquid flows. In order to test the method and also visualize the effect of the interaction between the different interfacial length scales, a "quasi-slug" flow was analyzed. The "quasi-slug" flow is a fabricated flow pattern created by the injection of a Taylor bubble (large scale interface length) in a bubbly flow (small-scale interface length) stream. The PTV tracking is based on the enhancement of algorithms found in the literature. Additionally, the PTV described in this work is capable of capturing the Taylor bubble nose shape, which can be used in further investigations. From the coupled PTV algorithm proposed here, it was possible to acquire Eulerian ensemble averaged fields of the dispersed bubble velocities and other properties around the Taylor bubbles. The results show that the bubbly flow stream void fraction significantly alters the Taylor bubble nose velocity in different liquid superficial velocity conditions. From the $\langle v_g \rangle$ Eulerian fields, it was possible to visualize that the wake recirculation near the Taylor bubble bottom gets stronger as the global void increases, as indicated by the dispersed bubble vertical average velocity Eulerian field. The image processing techniques and the PTV developed in this work can further used to investigate the small and large interfacial length interaction which occurs on real slug flows.

## 5. ACKNOWLEDGEMENTS

This work was realized with the financial support of PETROBRAS, through the Human Resources Program PFRH.

## 6. REFERENCES

Acuña, C.A. and Finch, J.A., 2010. "Tracking velocity of multiple bubbles in a swarm". *International Journal of Mineral Processing*, Vol. 94, No. 3-4, pp. 147–158. ISSN 03017516. doi:10.1016/j.minpro.2010.02.001.

Bugg, J.D. and Saad, G.A., 2002. "The velocity field around a Taylor bubble rising in a stagnant viscous fluid: Numerical and experimental results". *International Journal of Multiphase Flow*, Vol. 28, No. 5, pp. 791–803. ISSN 03019322. doi:10.1016/S0301-9322(02)00002-2.

Cerqueira, R., Paladino, E., Ynumaru, B. and Maliska, C., 2018. "Image processing techniques for the measurement of two-phase bubbly pipe flows using particle image and tracking velocimetry (piv/ptv)". *Chemical Engineering Science*.

Fu, Y. and Liu, Y., 2016. "Development of a robust image processing technique for bubbly flow measurement in a narrow rectangular channel". *International Journal of Multiphase Flow*, Vol. 84, pp. 217–228. ISSN 03019322. doi:10.1016/j.ijmultiphaseflow.2016.04.011.

Honkanen, M., Saarenrinne, P., Stoor, T. and Niinimäki, J., 2005. "Recognition of highly overlapping ellipse-like bubble images". *Meas. Sci. Technol. Meas. Sci. Technol*, Vol. 16, No. 16, pp. 1760–1770. doi:10.1088/0957-0233/16/9/007.

Lau, Y., Deen, N. and Kuipers, J., 2013. "Development of an image measurement technique for size distribution in dense bubbly flows". *Chemical Engineering Science*, Vol. 94, pp. 20–29. ISSN 00092509. doi:10.1016/j.ces.2013.02.043.

Mayor, T.S., Pinto, A.M.F.R. and Campos, J.B.L.M., 2007. "An image analysis technique for the study of gas-liquid slug flow along vertical pipes - associated uncertainty". *Flow Measurement and Instrumentation*, Vol. 18, No. 3-4, pp. 139–147. ISSN 09555986. doi:10.1016/j.flowmeasinst.2007.05.004.

Meneghini, C., Paladino, E., Brito, R. and Maliska, C., 2014. "Piv measurements of the flow around taylor bubbles in the presence of small dispersed bubbles". In *15th Brazilian Congress of Thermal Sciences and Engineering*.

Nogueira, S., Riethmuller, M.L., Campos, J.B. and Pinto, A.M., 2006. "Flow patterns in the wake of a Taylor bubble rising through vertical columns of stagnant and flowing Newtonian liquids: An experimental study". *Chemical Engineering Science*, Vol. 61, No. 22, pp. 7199–7212. ISSN 00092509. doi:10.1016/j.ces.2006.08.002.

Nogueira, S., Sousa, R.G., Pinto, A.M., Riethmuller, M.L. and Campos, J.B., 2003. "Simultaneous PIV and pulsed shadow technique in slug flow: A solution for optical problems". *Experiments in Fluids*, Vol. 35, No. 6, pp. 598–609. ISSN 07234864. doi:10.1007/s00348-003-0708-8.

Polonsky, S., Barnea, D. and Shemer, L., 1999. "Averaged and time-dependent characteristics of the motion of an elongated bubble in a vertical pipe". *International Journal of Multiphase Flow*, Vol. 25, No. 5, pp. 795–812. ISSN 03019322.

Van Hout, R., Gulitski, A., Barnea, D. and Shemer, L., 2002. "Experimental investigation of the velocity field induced by a Taylor bubble rising in stagnant water". *International Journal of Multiphase Flow*, Vol. 28, No. 4, pp. 579–596. ISSN 03019322. doi:10.1016/S0301-9322(01)00082-9.

Xue, T., Qu, L., Cao, Z. and Zhang, T., 2012. "Three-dimensional feature parameters measurement of bubbles in gas-liquid two-phase flow based on virtual stereo vision". *Flow Measurement and Instrumentation*, Vol. 27, pp. 29–36. ISSN 09555986. doi:10.1016/j.flowmeasinst.2012.07.007.

## 7. RESPONSIBILITY NOTICE

The authors are the only responsible for the printed material included in this paper.